



In Situ Synthesis of ZnCo₂O₄ and Pd@ZnCo₂O₄ Nanocomposites for Dye Degradation and Biological Applications

Supriya Gumma^{1,2}, Puthalapattu Reddy Prasad^{3*}, Sandhya Punyasamudram², Adikay Sreedevi², Venkata Nagendra Kumar Putta¹ and Phani Raja Kanuparth¹

¹Department of Chemistry, GITAM School of Sciences, GITAM (Deemed to be University), Hyderabad, TG, India

²Department of Chemistry, Sri Padmavathi Mahila Visvavidyalayam, Tirupati, AP, India

³Department of Chemistry, Institute of Aeronautical Engineering, Dundigal, Hyderabad, TG, India

Received: 07.07.2024 Accepted: 05.08.2024 Published: 30.09.2024

*prasadchem@gmail.com

ABSTRACT

In this study, ZnCo₂O₄ and Pd@ZnCo₂O₄ were synthesized through a novel phytochemical process using the leaf extract of *Catharanthus roseus* for photocatalytic and biological applications. The synthesized nanoparticles were characterized through X-ray diffraction, scanning electron microscopy, energy-dispersive X-ray spectroscopy, Fourier-transform infrared spectroscopy, and UV-Visible spectroscopy. The photocatalytic activities of ZnCo₂O₄ and Pd@ZnCo₂O₄ (10 mg) were evaluated after 40 min of reaction by degrading brilliant blue dye (100 µg/mL solution), achieving 42% and 97% degradation, respectively. This green synthesis method for ZnCo₂O₄ and Pd@ZnCo₂O₄ proves to be an eco-friendly, modest, and effective approach for the photodegradation of brilliant blue dye in an aqueous medium. Additionally, the ZnCo₂O₄ and Pd@ZnCo₂O₄ catalysts were also tested for their antibacterial and antioxidant activities.

Keywords: *Catharanthus roseus*; Synthesis; Photodegradation; ZnCo₂O₄; Brilliant blue.

1. INTRODUCTION

Nanotechnology is a rapidly advancing field of research that has achieved significant success in modern technology (Femina *et al.* 2024; Debasis *et al.* 2023). Nanoparticles, typically ranging in size from 1 to 100 nm, exhibit diverse properties in terms of structure, physicochemical characteristics, electrical, magnetic, thermal, mechanical, catalytic, optical scattering, and shape (Jiajun *et al.* 2024; Hafsah *et al.* 2024). Metals and metal oxides have numerous applications in areas such as pollutant detection, remediation, photodegradation, water treatment, catalysis, electronics, cancer therapy, drug delivery, and tissue repair (Ayush *et al.* 2024; Rashmi *et al.* 2023). Traditional methods of nanoparticle synthesis, such as pyrolysis and abrasion, have notable drawbacks, including high costs, low synthesis rates, and substantial energy requirements (Madhuree *et al.* 2023).

Chemical methods like sol-gel technology and chemical reduction are also commonly used but involve toxic substances and generate hazardous byproducts (Prasad *et al.* 2016). Consequently, there is a persistent interest in the scientific community to develop safer, environmentally friendly, cost-effective, and cleaner nanoparticle synthesis techniques (Akbar *et al.* 2023; Siyuan *et al.* 2023). Recent research has focused on the synthesis of metal oxide nanoparticles using various

plant extracts (Mohammed *et al.* 2024; Uyiosa *et al.* 2024). The biogenic production of metal and metal oxide nanoparticles is gaining popularity due to its simple experimental setup and the ability to obtain nanoparticles of different sizes and morphologies easily (Kok *et al.* 2024; Aynur *et al.* 2024).

Metal oxide nanoparticles can be biologically synthesized using live organisms such as plants, bacteria, algae, actinomycetes, viruses, and fungi. This biosynthesis process utilizes a universal solvent and produces nanoparticles free of toxic chemical contaminants, making them well-suited for biomedical applications. The natural synthesis process involves two key steps: bio-reduction and biosorption (Arighna *et al.* 2024). Bio-reduction refers to the chemical reduction of metal ions into stable forms, while biosorption involves the attachment of metal ions to the surfaces of organisms, such as cell walls and peptides, to form stabilized complexes (Mouhaned *et al.* 2024). Additionally, biologically active molecules can attach to or cap the nanoparticles, producing stable particles (Vinod *et al.* 2023). These biobased synthesis methods are typically faster than physicochemical approaches (Amin *et al.* 2023; Rosa *et al.* 2024; Mohammad *et al.* 2024). Transition metal oxides with a spinel structure have attracted significant interest due to their unique magnetic, electrical, and optical properties. The conventional

chemical formula for spinel, AB_2O_4 , represents divalent and trivalent metal ions arranged in tetrahedral and octahedral positions, respectively (Monireh *et al.* 2024).

Spinel $ZnCo_2O_4$ is a metal oxide utilized in energy applications due to its unique properties, such as protective coating applications and magnetic hysteresis behaviour (Sabahat *et al.* 2023; Sebastian *et al.* 2024). Various techniques can be employed to synthesize zinc cobalt oxide, including the sol-gel method, co-precipitation approach, oxide powders milling, spray pyrolysis, and green synthesis method (Flores *et al.* 2022; Huaxing *et al.* 2024). Transition metal oxides hold great promise as photocatalysts for environmental applications due to their affordability, ease of synthesis, and strong activity in alkaline solutions (Tholkappiyan *et al.* 2024; Eneyew *et al.* 2024; Pore *et al.* 2024). Specifically, spinel oxides containing metal elements with variable valence states, such as $MnCo_2O_4$ (Nada *et al.* 2022), $NiCo_2O_4$ (Shankar *et al.* 2024), and Co_3O_4 (Jothirathinam *et al.* 2023) offer high catalytic activity for energy applications (Maha *et al.* 2022).

To further enhance the catalytic performance of spinel oxides, various strategies have been employed, including structure design, morphological control, and electronic structure regulation (Varunamugi *et al.* 2024). Oxygen vacancies, a type of cation defect, play a crucial role in improving the catalytic activity of transition metal oxides by adjusting their electronic structure. The catalyst, $ZnCo_2O_4$ is considered as a potential semiconductor material due to its numerous advantages, such as high conductivity, low cost, environmental friendliness, and high theoretical capacitance (Rui *et al.* 2023). Various nanostructures of $ZnCo_2O_4$, including nanowires (Zikirina *et al.* 2021), nanosheets (Bo *et al.* 2024), nanoparticles (Priya *et al.* 2019), and nanospheres (Sunaina *et al.* 2023), have been synthesized to leverage its properties.

In this study, $ZnCo_2O_4$ and $Pd@ZnCo_2O_4$ nanoparticles were synthesized using a novel green method involving the extract from *Catharanthus roseus* leaves. The synthesized nanocomposites were characterized through various methods, and their antibacterial properties were evaluated against specific Gram-positive and Gram-negative bacterial species. Additionally, the nanoparticles were used to catalyze the photodegradation of brilliant blue in an aqueous phase and were tested for their antibacterial and antioxidant activities.

2. EXPERIMENTAL SECTION

2.1 Materials and Methods

The following analytical reagents were utilized in this investigation: zinc chloride ($ZnCl_2$), cobalt chloride ($CoCl_2 \cdot 6H_2O$), palladium chloride ($PdCl_2$), and

ascorbic acid; all were obtained from Sigma-Aldrich. All other chemicals used were of analytical grade and were used as received without any further purification. Ultrapure water was employed to prepare aqueous stock solutions.

2.2 Characterization

The synthesized $ZnCo_2O_4$ and $Pd@ZnCo_2O_4$ nanoparticles were characterized using several analytical techniques. The crystal structure of the synthesized nanoparticles was analyzed using a Bruker D8 Advanced X-ray powder diffractometer (XRD), scanning the 2θ range from 0 to 80° at a rate of 2° per minute, with standard Cu-K α radiation ($\lambda = 1.54 \text{ \AA}$). The morphology of the nanoparticles was examined using a field emission scanning electron microscope (JEOL, JSM-7610F PLUS) equipped with energy dispersive X-ray analysis. FTIR spectroscopy was used to identify functional groups associated with biomolecules, with infrared analysis performed in the $400\text{--}4000 \text{ cm}^{-1}$ range (Perkin Elmer FTIR Spectroscopy). A Shimadzu UV-1800 UV-Visible spectrophotometer was used to measure the optical properties of the catalyst and reaction mixture.

2.3 Plant Extract Preparation

Plant leaves were collected from the vicinity of Gitam University, Hyderabad. These leaves were thoroughly washed with both tap and distilled water and then dried under sunlight for two days. Once dried, the leaves were ground into a powder using a grinder. About 50 grams of *Catharanthus roseus* leaf powder was then dispersed in 100 mL of distilled water, stirred, and heated to 70°C for 60 min. The mixture was allowed to cool to room temperature before being filtered through Whatman filter paper No.1 and stored at 4°C for future experimental use.

2.4 Synthesis of $ZnCo_2O_4$ and $Pd@ZnCo_2O_4$ Nanocatalysts

To prepare the $ZnCo_2O_4$ composite, a 1:2 molar ratio of $ZnCl_2$ and $CoCl_2 \cdot 6H_2O$ was dissolved in 50 mL of distilled water and stirred for 30 min. Dropwise addition of the prepared plant extract was followed by constant stirring until the suspension was uniform. The temperature of the suspension was maintained between $70\text{--}80^\circ \text{C}$ for 4 hours. The resulting dark brown precipitate was filtered and washed with ethanol and distilled water, then dried at room temperature. The dried samples were subsequently calcined in a hot air oven at 400°C for 3 hours, resulting in the formation of black, porous $ZnCo_2O_4$. The same procedure was followed to synthesize $Pd@ZnCo_2O_4$ nanocomposites, with the addition of a 0.5 mole ratio of $PdCl_2$ solution.

2.5 Photo-catalytic Activity

The synthesized ZnCo_2O_4 and $\text{Pd@ZnCo}_2\text{O}_4$ nanoparticles were evaluated as catalysts for the photodegradation of brilliant blue dye. A 50 mL solution containing 100 $\mu\text{g}/\text{mL}$ of the dye was prepared in a beaker, to which 10 mg of the catalyst (either ZnCo_2O_4 or $\text{Pd@ZnCo}_2\text{O}_4$) was added. The mixture was stirred in the dark for 30 min to reach adsorption equilibrium. Following this, the reaction mixture was exposed to UV-Visible light using a 100 W incandescent light bulb. Samples of 1 mL were taken at regular intervals, and their absorption spectra were measured using a UV-Visible absorption spectrophotometer.

2.6 Antibacterial Activity

The antibacterial effectiveness of green-synthesized ZnCo_2O_4 , $\text{Pd@ZnCo}_2\text{O}_4$, and gentamicin (Gm) was evaluated against two pathogenic microorganisms: Gram-positive bacteria (*Staphylococcus aureus*) and Gram-negative bacteria (*Escherichia coli*). The agar well diffusion method (Punyasamudram *et al.* 2024) was employed to determine antibacterial activity. Each sample (10 mg/mL) was dissolved in 0.9% NaCl solution. Normal saline itself showed no antibacterial activity against the tested pathogens. Samples of 25 μl , 50 μl , and 100 μl of the green-synthesized nanocomposites (ZnCo_2O_4 and $\text{Pd@ZnCo}_2\text{O}_4$) and gentamicin were tested for antimicrobial activity. The standard control specimen, gentamicin, was applied to each plate (25 μl).

2.7 Antioxidant Activity

The antioxidant potential of green-synthesized ZnCo_2O_4 and $\text{Pd@ZnCo}_2\text{O}_4$ nanocomposites, along with *Catharanthus roseus* leaf extract, was assessed using the 2,2-diphenyl-1-picrylhydrazyl (DPPH) assay. In this method, 1 mL of 0.1 mM DPPH solution was added with 3 mL of the nanocomposites, and the plant extract was dissolved in ethanol at varying concentrations (2.0, 4.0, 8.0, 16.0, 32.0, 64.0, 128, 256, 512, 1024 $\mu\text{g}/\text{mL}$), prepared by dilution. Ascorbic acid was used as a standard, and a DPPH solution without any sample was prepared as a control. The mixture was vigorously shaken and left at room temperature for 30 min for record the absorbance using a spectrophotometer. The assay was performed in triplicate, and the IC_{50} value was determined from the logarithmic dose inhibition curve. The percentage of DPPH scavenging effect was calculated using the formula:

$$(\%) \text{ DPPH Scavenging effect} = A_0 - A_t / A_0 \times 100$$

where, A_0 was the absorbance of the control reaction and A_t was the absorbance in the presence of test.

3. RESULTS AND DISCUSSION

The synthesized ZnCo_2O_4 and $\text{Pd@ZnCo}_2\text{O}_4$ nanoparticles were dispersed in ultrapure water and subjected to 10 min of sonication for UV-Visible spectral analysis (Fig. 1). The UV-Visible spectrum of the plant extract exhibited absorption peaks at 272 nm and 316 nm, indicating the presence of phenolic compounds, as depicted in Fig. 1a. Furthermore, distinct UV-Visible absorption bands were observed to diminish and were replaced by prominent new absorption peak in the 250-350 nm range, confirming the successful synthesis of ZnCo_2O_4 and $\text{Pd@ZnCo}_2\text{O}_4$ nanoparticles using an aqueous extract of *Catharanthus roseus*, as shown in Fig. 1b and Fig. 1c. This absorption band is attributed to the oscillation of electrons in the conduction band induced by the electromagnetic field. Notably, $\text{Pd@ZnCo}_2\text{O}_4$ exhibited an additional surface plasmon absorption band at 350 nm, distinctive to palladium, evident in the UV-Visible spectrum (Fig. 1c) (Sandhya *et al.* 2023).

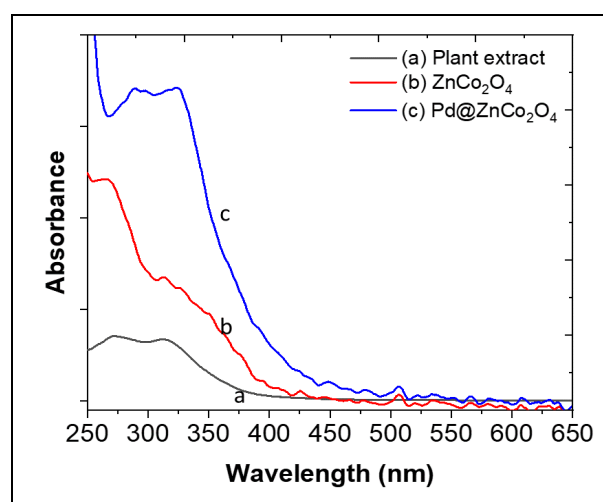


Fig. 1: UV-visible spectra of (a) plant extract (b) ZnCo_2O_4 and (c) $\text{Pd@ZnCo}_2\text{O}_4$ spinel nanocomposites

FT-IR analysis was conducted to identify various functional groups present in the leaf extract of *Catharanthus roseus*, which contribute to the synthesis of nanoparticles and serve as capping and stabilizing agents. The FTIR spectra of the plant extract (Fig. 2a) and the synthesized nanocomposites of ZnCo_2O_4 (Fig. 2b) and $\text{Pd@ZnCo}_2\text{O}_4$ (Fig. 2c) are illustrated in Fig. 2. In Fig. 2a, a distinct peak at 3450.24 cm^{-1} corresponds to the hydroxyl group characteristic of phenolic compounds. Other significant peaks include 1630.18 cm^{-1} (carbonyl group), 1380.74 cm^{-1} (amide group), 1082.24 cm^{-1} and $(\text{C}-\text{O}$ of alcohols or phenols) are corresponding to plant extract. In Fig. 2b and Fig. 2c, the peaks at 3323.35 cm^{-1} indicates the O-H stretching vibration of adsorbed water molecules on the nanomaterial surface both spectra exhibit similar peaks, with slight shifts and broadening observed in the peaks of the plant extract containing nanoparticles. Additionally, absorption bands at 660.42

cm^{-1} and 570.40 cm^{-1} correspond to the stretching vibrations of Zn-O and Co-O, respectively (Sandhya *et al.* 2023).

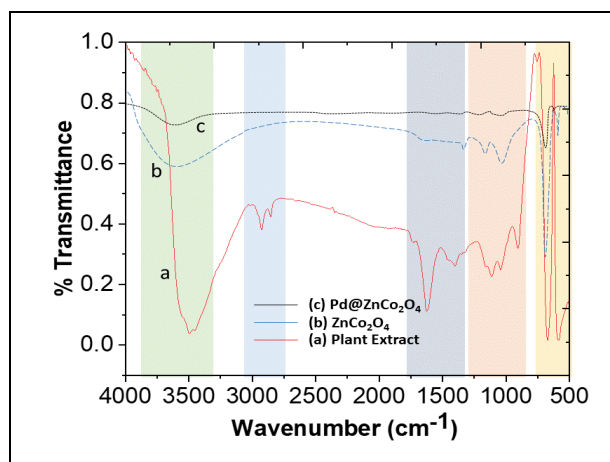


Fig. 2: FTIR spectra of (a) plant extract (b) ZnCo_2O_4 and (c) $\text{Pd@ZnCo}_2\text{O}_4$ spinel nanocomposites

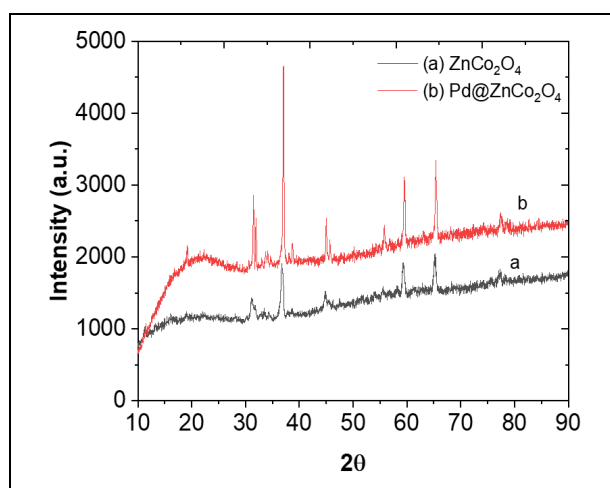


Fig. 3: XRD pattern of ZnCo_2O_4 and $\text{Pd@ZnCo}_2\text{O}_4$ spinel nanocomposites

The successful green synthesis of ZnCo_2O_4 and $\text{Pd@ZnCo}_2\text{O}_4$ nanoparticles was confirmed by XRD spectroscopy, with the XRD patterns presented in Fig. 3. These patterns exhibit sharp peaks indicative of the crystalline nature of the synthesized materials. In the XRD pattern of ZnCo_2O_4 , prominent peaks are observed at 2θ values of 31° , 37° , 44° , 55° , 59° , 65° , and 77° , corresponding to the (220), (311), (400), (422), (511), (511), and (440) planes of the spinel crystalline phase (JCPDS 99-023-1390) (43). The XRD analysis of $\text{Pd@ZnCo}_2\text{O}_4$ reveals the coexistence of ZnCo_2O_4 and metallic Pd phases. Additional peaks at 2θ values of 39° and 46° are attributed to Pd (Do *et al.* 2014). These findings indicate that metallic Pd nanoparticles are distributed within the ZnCo_2O_4 matrix. The XRD patterns also show that the Pd-modified ZnCo_2O_4 sample exhibits enhanced crystallinity, higher intensity, and

narrower peak widths compared to pure ZnCo_2O_4 . The crystallite sizes were estimated using Scherrer's formula based on the full width at half maximum from the XRD patterns, yielding average sizes of approximately $\sim 26.4 \text{ nm}$ for ZnCo_2O_4 and 22.5 nm for $\text{Pd@ZnCo}_2\text{O}_4$ across all peaks (Sandhya *et al.* 2023). The absence of additional peaks in the XRD patterns confirms the purity of the synthesized products.

The morphology of green-synthesized ZnCo_2O_4 and $\text{Pd@ZnCo}_2\text{O}_4$ nanoparticles was investigated using SEM, as depicted in Fig. 4. Figs. 4 (A-D) present FE-SEM images of ZnCo_2O_4 and $\text{Pd@ZnCo}_2\text{O}_4$ nanoparticles at various magnifications, revealing irregular shapes and rough particles with a size distribution ranging from 10 to 25 nm. The SEM micrographs illustrate that the particles are irregular, granular, heterogeneous, non-agglomerated, and dispersed in nature. The rough surface of the synthesized nanoparticles enhances their potential for environmental applications by facilitating better interaction with bacterial cell walls and pollutants (Sandhya *et al.* 2023).

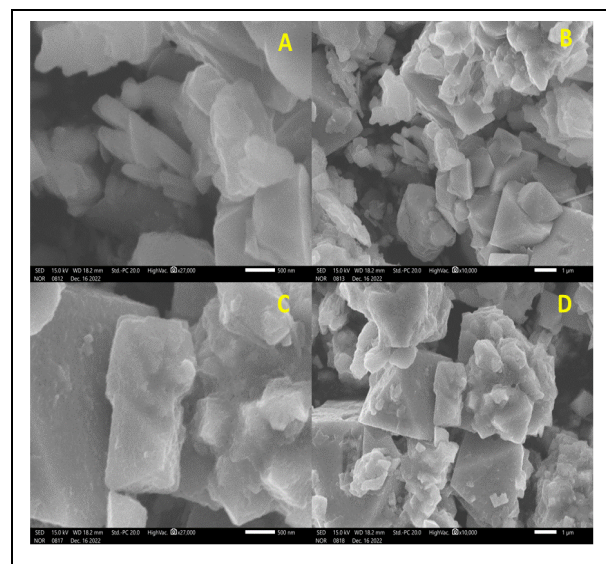


Fig. 4: FE-SEM image of ZnCo_2O_4 (A and B) and $\text{Pd@ZnCo}_2\text{O}_4$ (C and D) spinel nanocomposites

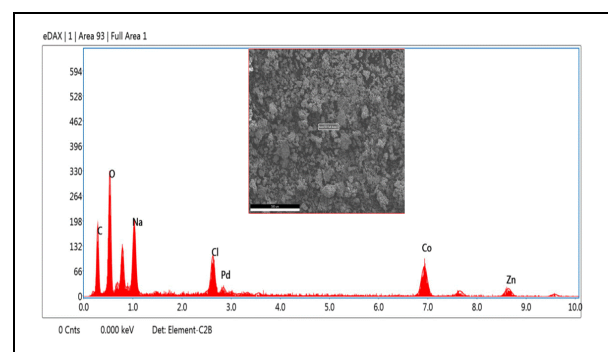


Fig. 5: EDX spectrum of ZnCo_2O_4 and $\text{Pd@ZnCo}_2\text{O}_4$ nanocomposites

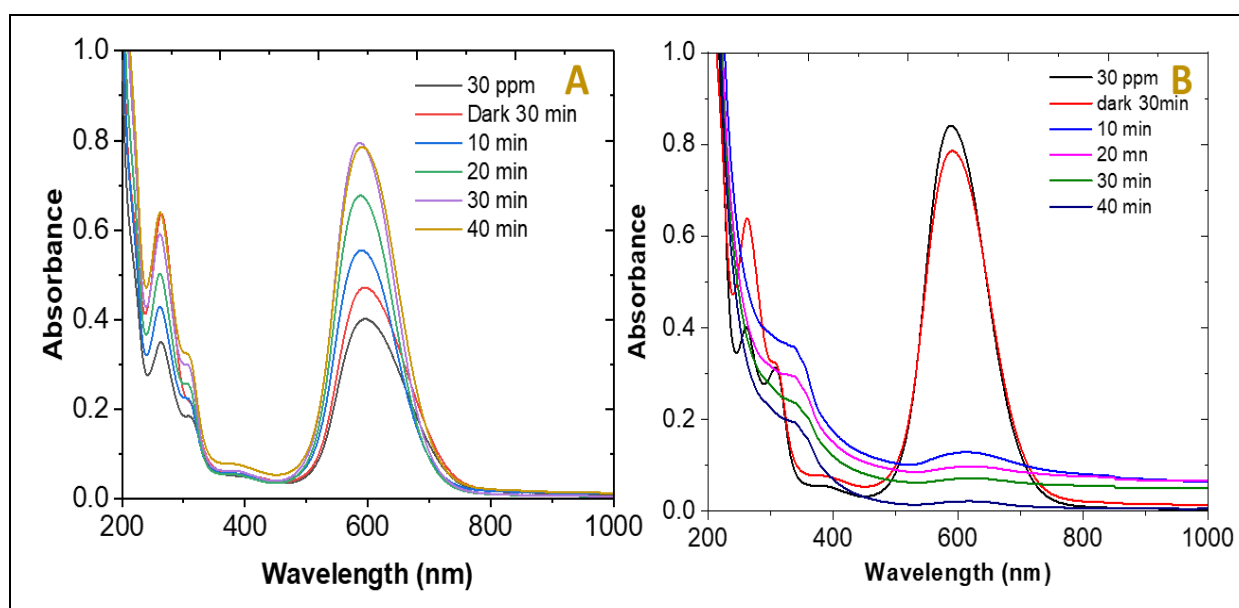


Fig. 6: UV-Visible spectra of brilliant blue solution irradiated with UV light at different time intervals in the presence of (A) ZnCo_2O_4 and (B) $\text{Pd@ZnCo}_2\text{O}_4$ nanocomposites

The elemental composition of the synthesized ZnCo_2O_4 and $\text{Pd@ZnCo}_2\text{O}_4$ nanocomposites was analyzed by (EDX), as shown in Fig. 5. The major peaks in the EDX spectrum confirm the presence of Co and O in the nanoparticles. Minor peaks of carbon, and chlorine are also observed, attributed to residues from the plant extract used in synthesis. The EDX analysis indicates that the nanoparticles consist of approximately 26 wt% cobalt and 68 wt% oxygen, consistent with cobalt oxide (ZnCo_2O_4). The elemental composition data from EDX align well with theoretically calculated values, indicating uniform composition of the nanoparticles. The EDX spectrum shows sharp peaks corresponding to crystalline ZnCo_2O_4 and $\text{Pd@ZnCo}_2\text{O}_4$ nanocomposites in the energy range of 1.0-9.0 KeV.

3.1 Photo-catalytic Activity

The photocatalytic degradation of brilliant blue was investigated using ZnCo_2O_4 and $\text{Pd@ZnCo}_2\text{O}_4$ as catalysts under UV-Visible light irradiation. It was observed that 42% and 97% of a 50 mL solution (100 mg/L initial concentration) of brilliant blue degraded within 40 min when catalyzed by 10 mg of $\text{Pd@ZnCo}_2\text{O}_4$ at room temperature. The UV-Visible spectrum of the treated dye solution, shown in Fig. 6, indicates a reduction in absorbance at λ_{max} (602 nm) with increasing reaction time, demonstrating the photocatalytic degradation of brilliant blue. These experiments confirm that $\text{Pd@ZnCo}_2\text{O}_4$ exhibits superior efficiency in degrading brilliant blue in aqueous solutions.

Comparative analysis of the photocatalytic activities of ZnCo_2O_4 and $\text{Pd@ZnCo}_2\text{O}_4$ is presented in Figs. 6A & 6B. The degradation of the dye occurs through the generation of electrons and holes on the catalyst surface under light irradiation. These reactive species, particularly $\cdot\text{OH}$ radicals, oxidize the dye molecules into simpler inorganic compounds.

The addition of Pd enhances the photocatalytic performance of ZnCo_2O_4 by suppressing the recombination of photo-generated electrons and holes (Sandhya *et al.* 2023). The photocatalytic degradation kinetics of green-synthesized ZnCo_2O_4 and $\text{Pd@ZnCo}_2\text{O}_4$ can be described using a pseudo-first-order kinetics model, $\ln(C/\text{Co}) = kt$, where k is the rate constant of the degradation process (Mohammed *et al.* 2023). Fig. 7 illustrates the kinetics of brilliant blue decomposition for the catalysts studied here, with measured rate constants (k) of 0.0027 min^{-1} for ZnCo_2O_4 and 0.0048 min^{-1} for $\text{Pd@ZnCo}_2\text{O}_4$ nanocomposites (Fig. 8). Notably, $\text{Pd@ZnCo}_2\text{O}_4$ exhibits a significantly higher rate constant, approximately 2.5 times greater than that of pure ZnCo_2O_4 , underscoring its enhanced photocatalytic activity. A comparative analysis of the photocatalytic performance of $\text{Pd@ZnCo}_2\text{O}_4$ for the degradation of brilliant blue against other catalysts reported in the literature is presented in Table 1. This comparison highlights the superior efficacy of $\text{Pd@ZnCo}_2\text{O}_4$ nanocomposites compared to previously reported catalysts.

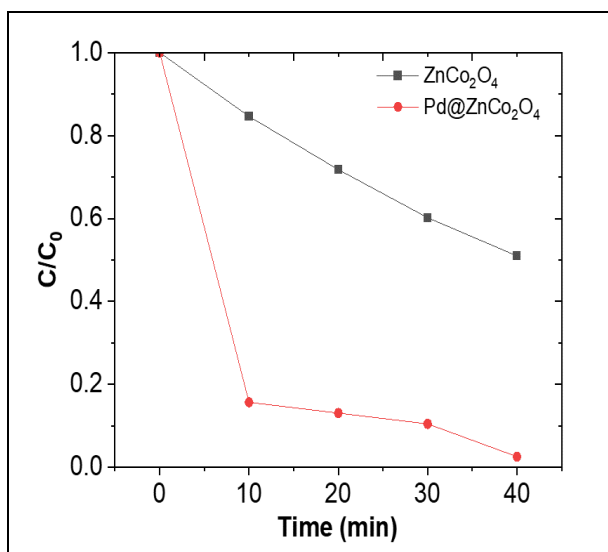


Fig. 7: Kinetic study of (A) $ZnCo_2O_4$ and (B) $Pd@ZnCo_2O_4$ nanocomposites

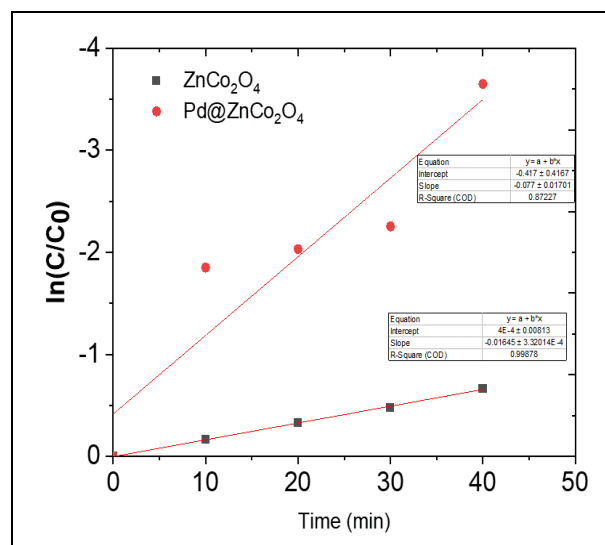


Fig. 8: Pseudo-first-order kinetics of photo-catalytic degradation of brilliant blue in UV-Visible light

Table 1. A comparison of the photo-catalytic degradation of pollutants

Photocatalyst	Method	Catalyst loading	Degradation Time (min)	Degradation Efficiency (%)	References
Au@ZnO-Pd	Reduction	1 mg	20	84	Li <i>et al.</i> (2017)
ZnO/Au/Pd	Photo-deposition	5 mg	180	97	Seung <i>et al.</i> (2019)
TiO ₂ /Pd	-	20 mg	20	95	Khalid <i>et al.</i> (2017)
ZnO-CdS/Pd	Hydrothermal	-	30	86.6	Mohwes <i>et al.</i> (2023)
$Pd@Zn_2Co_2O_4$	Green synthesis	10 mg	45	97	Present work

Table 2. Antibacterial activity of $ZnCo_2O_4$ and $Pd@ZnCo_2O_4$ nanoparticles

Bacterial strains	Zone of inhibition (mm)							
	$ZnCo_2O_4$			Gm		$Pd@ZnCo_2O_4$		Gm
	25 μ L	50 μ L	100 μ L	25 μ L	25 μ L	50 μ L	100 μ L	25 μ L
<i>E. coli</i>	6.8	7.2	7.6	6.6	6.6	7.2	8.2	6.4
<i>S. aureus</i>	3.2	4.4	4.6	4.8	3.5	4.2	4.8	5.6

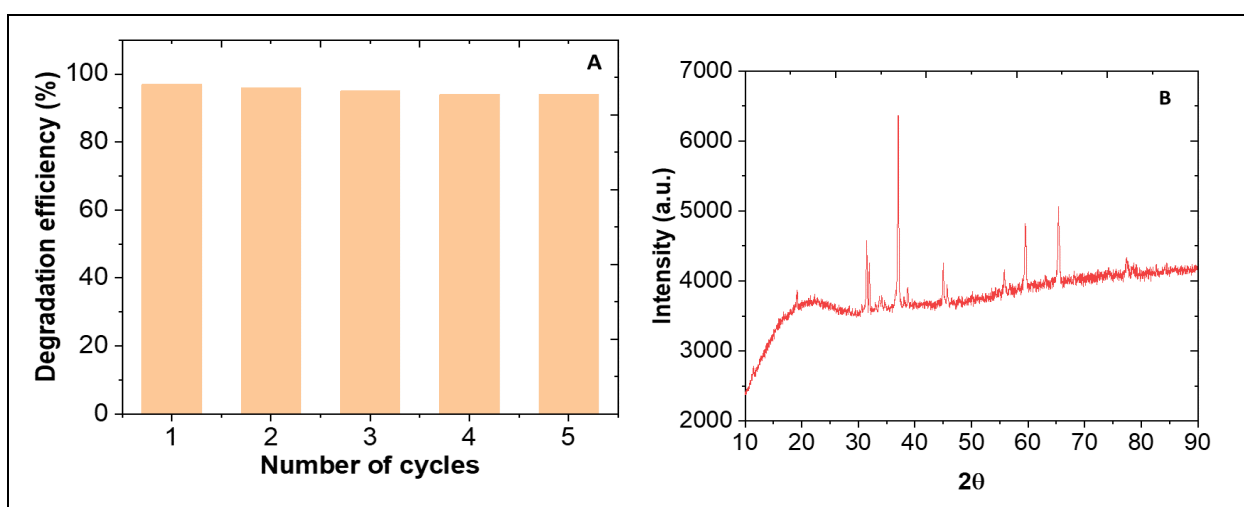


Fig. 9: (A) Degradation efficiency after five cycles (B) XRD pattern of $Pd@ZnCo_2O_4$ nanocomposites after photo-catalytic process

3.2 Recyclability and Reusability

The ability to reuse photocatalysts is crucial for their practical application. Hence, the recyclability of the photocatalyst was evaluated over five cycles of the photocatalysis process. It was found that there was a minimal reduction in the photocatalytic degradation efficiency of Pd@ZnCo₂O₄ nanoparticles, as illustrated in Fig. 9A. Additionally, XRD analysis conducted after the photocatalysis process indicated that the crystal structure of Pd@ZnCo₂O₄ remained unchanged compared to its state before the photocatalytic process, as depicted in Fig. 9B.

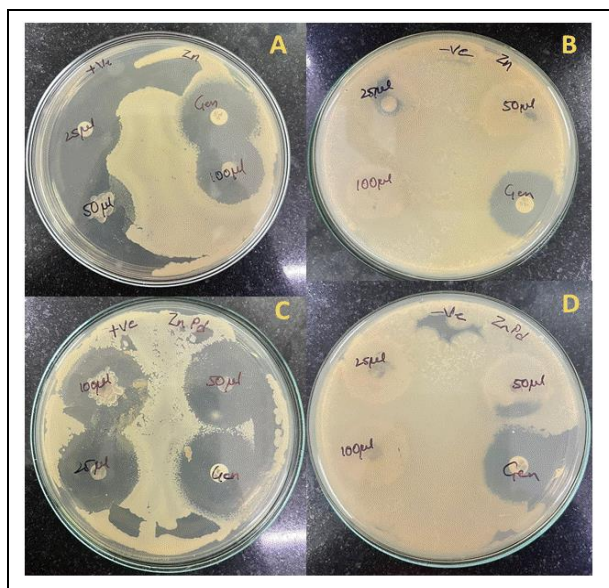


Fig. 10: Antimicrobial activity of the green synthesized ZnCo₂O₄ (A and B) and Pd@ZnCo₂O₄ (C and D)

3.3 Antibacterial Activity

Table 2 presents the findings from the antibacterial assessment of green-synthesized ZnCo₂O₄ and Pd@ZnCo₂O₄ nanoparticles and gentamicin (Gm) against two different pathogenic microorganisms. The results indicate that both ZnCo₂O₄ and Pd@ZnCo₂O₄ nanoparticles exhibited significant inhibition zones against *E. coli*, with the latter showing the highest inhibition (Fig. 10). The ZnCo₂O₄ and Pd@ZnCo₂O₄ nanoparticles demonstrated notable antibacterial efficacy compared to the conventional antibiotic gentamicin. The antibacterial mechanism of phytochemicals involves disrupting the cellular membrane, leading to cell death, consistent with previous reports (Layth *et al.* 2024). Meanwhile, the mechanism of action of ZnCo₂O₄ and Pd@ZnCo₂O₄ nanoparticles entails binding to and interacting with the cell membrane, accumulating in the lipid layer, and inhibiting enzymes, DNA, and ATP synthesis, ultimately causing cell lysis.

3.4 Antioxidant Activity

A study of the antioxidant capacity of the green synthesized ZnCo₂O₄ and Pd@ZnCo₂O₄ was carried out by using the DPPH as illustrated in Fig. 11. The results shows that Pd@ZnCo₂O₄ nanoparticles have significant antioxidant properties, scavenging free radicals in a dose-dependent manner. The scavenging potential of the ZnCo₂O₄ and Pd@ZnCo₂O₄ nanoparticles is consistently less effective than that of the standard. DPPH activity of 84.2%, 66.4%, and 75.6% were observed respectively for *Catharanthus roseus* extract, ZnCo₂O₄ and Pd@ZnCo₂O₄ nanoparticles at 1024 g/mL. In this study, the IC₅₀ of Pd@ZnCo₂O₄ was 70.5 µg/mL, indicating greater activity than the photosynthesized ZnCo₂O₄ nanoparticles. This increased activity is likely attributed to the presence of more secondary metabolites and a higher concentration of phenolic hydroxyl groups in their structure (Hamdullah *et al.*, 2022). Additionally, phenolic and terpenoid compounds, which are known for their strong antioxidant properties, acted as capping agents for ZnCo₂O₄ and Pd@ZnCo₂O₄ nanoparticles, potentially enhancing their antioxidant activity (Rahman *et al.*, 2024).

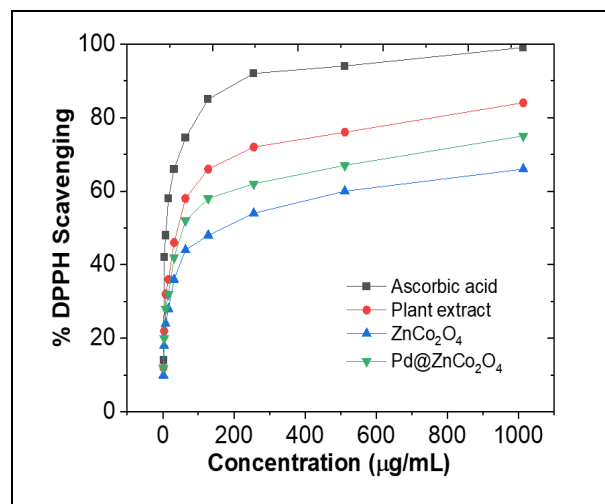


Fig. 11: Antioxidant activity of ascorbic acid, plant leaf extract, ZnCo₂O₄ and Pd@ZnCo₂O₄ nanoparticles

4. CONCLUSION

Here, ZnCo₂O₄ and Pd@ZnCo₂O₄ were successfully synthesized using eco-friendly and cost-effective phytochemical methods with *Catharanthus roseus* leaf extract. The photocatalytic activities of the synthesized particles were evaluated by degrading brilliant blue under UV light irradiation. Results showed that 46% and 97% degradation of brilliant blue was achieved within 40 min of irradiation using ZnCo₂O₄ and Pd@ZnCo₂O₄ as catalysts, respectively. The reaction mechanism followed a pseudo-first-order kinetics model. The method is straightforward, economical, and environmentally friendly. It has the potential to be

applied to the synthesis of other metal and metal oxides nanoparticles. As a result of the use of biological sources in synthesis, nanoparticles are gaining a new dimension in all aspects of their application.

FUNDING

There is no funding source.

CONFLICT OF INTEREST

The authors declared no conflict of interest in this manuscript regarding publication.

COPYRIGHT

This article is an open-access article distributed under the terms and conditions of the Creative Commons Attribution (CC BY) license (<http://creativecommons.org/licenses/by/4.0/>).



REFERENCES

- Akbar, K. I., Rutuja, S. R., Nitin, R. H., Ashok, S. K., Bapusaheb, H. S., Shashikant, P. P., Satish, B. S. and Shaikatali, N. I., A review on environmental applications of metal oxide nanoparticles through waste water treatment, *Mater. Today Proc.*, (2023) <https://doi.org/10.1016/j.matpr.2023.05.527>
- Amin, S. D., Seyed, S. H., Majid, R. A., Mahin, N. and Naghmeh, S., Mentha pulegium as a source of green synthesis of nanoparticles with antibacterial, antifungal, anticancer, and antioxidant applications, *Sci. Hortic.*, 320, 112215 (2023). <https://doi.org/10.1016/j.scienta.2023.112215>
- Arighna, S., Prashant, M., Goutam, B. and Snehasis, B., Greening the pathways: a comprehensive review of sustainable synthesis strategies for silica nanoparticles and their diverse applications, *RSC Adv.*, 14(16), 11197-11216 (2024). <https://doi.org/10.1039/d4ra01047g>
- Aynur, Ş., Şakir, A. and Kadriye, K., An approach for cationic dyes removal from wastewater: Green synthesis of iron nanoparticles using Prunus avium stems extracts, *Kuwait J. Sci.*, 51(3), 100226 (2024). <https://doi.org/10.1016/j.kjs.2024.100226>
- Ayush, B. and Jai, P., Noble metal nanoparticles and graphene oxide-based hybrid nanostructures for antibacterial applications: Recent advances, synergistic antibacterial activities, and mechanistic approaches, *Micro Nano Eng.*, 22, 100239 (2024). <https://doi.org/10.1016/j.mne.2024.100239>
- Bo, X., Ye, C., Qiyong, Z., Shouling, D. and Shiliu, Y., Controllable synthesis of ZnCo₂O₄@NiCo₂O₄ hierarchical nanosheets for high performance supercapacitors, *J. Phys. Chem. Solids*, 184, 111744 (2024). <https://doi.org/10.1016/j.jpics.2023.111744>
- Cheng, Z. Y., Siyu, H., Hongrui, Z., Jiang, L., Lunliang, Z., Yao, W., Tuck-Yun, C., Hong, Y., Xiaomeng, Z. and Shufeng, Y., Vacancy defect tuning of electronic structures of transition metal (hydr)oxide-based electrocatalysts for enhanced oxygen evolution, *Energy Adv.*, 2(1), 73-85 (2023). <https://doi.org/10.1039/d2ya00281g>
- Debasis, M., Priyanka, A., Rihab, D., Pooja, T., Kuldeep, J., Marika, P., Nurudeen, O. A., Bahman, K., Kamaljit, K., Ankita, P., Ansuman, S., Maddalena, D. G., Pradeep, K. D. M., Amaresh, K. N., Vijayakumar, S. and Periyasamy, P., Biosynthesis and characterization of nanoparticles, its advantages, various aspects and risk assessment to maintain the sustainable agriculture: Emerging technology in modern era science, *Plant Physiology and Biochemistry*, 196, 103-120 (2023). <https://doi.org/10.1016/j.plaphy.2023.01.017>
- Do, A. T. T., Giang, H. T., Do, T. T., Pham, N. Q. and Ho, G. T., Effects of palladium on the optical and hydrogen sensing characteristics of Pd-doped ZnO nanoparticles, *Beilstein J. Nanotechnol.* 5, 1261–1267 (2014). <https://doi.org/10.3762/bjnano.5.140>
- Eneyew, T. B., Yilikal, D. S., Bedasa, A. G., Fedlu, K. S., Mikyas, K. S., Ravikumar, C. R., Naveen, K., Ananda, M., Green synthesis of ternary ZnO/ZnCo₂O₄ nanocomposites using Ricinus communis leaf extract for the electrochemical sensing of sulfamethoxazole, *Inorg. Chem. Commun.*, 160, 111964 (2024). <https://doi.org/10.1016/j.inoche.2023.111964>
- Femina, C. C. and Kamalesh, T., Advances in stabilization of metallic nanoparticle with biosurfactants- a review on current trends, *Heliyon*, 10(9), e29773 (2024). <https://doi.org/10.1016/j.heliyon.2024.e29773>
- Flores-Lasluisa, J. X., Huerta, F., Cazorla-Amorós, D., Morallón, E., Transition metal oxides with perovskite and spinel structures for electrochemical energy production applications, *Environ. Res.*, 214(1), 113731 (2022). <https://doi.org/10.1016/j.envres.2022.113731>
- Hafsah, A., Fahad, H. A. Julie, M., Thomas, A., Jawwad, A. D., Ihtesham, U. R., Aqif, A. C. and Gwendolen, R., Synthesis of cerium, zirconium, and copper doped zinc oxide nanoparticles as potential biomaterials for tissue engineering applications, *Heliyon*, 10(7), e29150 (2024). <https://doi.org/10.1016/j.heliyon.2024.e29150>

- Hamdullah, S., Rima, N. E. T., Ismet, M., Aysenur, A., Meliha, K. G. and Fatih, S., An environmental approach for the photodegradation of toxic pollutants from wastewater using Pt–Pd nanoparticles: Antioxidant, antibacterial and lipid peroxidation inhibition applications, *Environ. Res.*, 208, 112708 (2022).
<https://doi.org/10.1016/j.envres.2022.112708>
- Hammed, M. L., Gulbagca, F., Nour, E. T. R., Aygun, A., Bekmezci, M. and Fatih, S., Hydrothermal-assisted synthesis of Co-doped ZnO nanoparticles catalyst for sodium borohydride dehydrogenation and photodegradation of organic pollutants in water, *Chem. Eng. J. Adv.*, 14, 100495 (2023).
<https://doi.org/10.1016/j.cej.2023.100495>
- Huaxing, L., Fafeng, X., Chunyang, M., Chaoyu, L., Magnetic field-assisted electrodeposition of ZnCo₂O₄-rGO nanoelectrodes for enhanced supercapacitor performance, *Chem. Eng. J.*, 152003 (2024).
<https://doi.org/10.1016/j.cej.2024.152003>
- Jiajun, W., Fengyu, G., Hengheng, L., Junyi, W., Tingkai, X., Honghong, Y., Yuansong, Z., Qingjun, Y., Shunzheng, Z. and Xiaolong, T., Metallic nanoparticles synthesized by algae: Synthetic route, action mechanism, and the environmental catalytic applications, *J. Environ. Chem. Eng.*, 12(1), 111742 (2024).
<https://doi.org/10.1016/j.jece.2023.111742>
- Jothirathinam, T., Muthukrishnan, F. P., Violet, D., Bavatharani, C., Jayakumar, P., Cyril, A. C. T., Annadurai, K. and Ragupathy, D., Facile synthesis of Co₃O₄@Se NPs grafted MWCNTs Nanocomposite for high energy density supercapacitor and antimicrobial applications, *Chem. Phys. Impact*, 7, 100253 (2023).
<https://doi.org/10.1016/j.chphi.2023.100253>
- Khalid, S., Idrees, K., Tamanna, G. and Mohammad, S., Efficient photodegradation of methyl violet dye using TiO₂/Pt and TiO₂/Pd photocatalysts, *Appl. Water Sci.*, 7, 3841–3848 (2017).
<https://doi.org/10.1007/s13201-017-0535-3>
- Kok, B. T., Daohua, S., Jiale, H., Tareque, O., Qingbiao, Li., State of arts on the bio-synthesis of noble metal nanoparticles and their biological application, *Chin. J. Chem. Eng.*, 30, 272-290, (2021).
<https://doi.org/10.1016/j.cjche.2020.11.010>
- Layth, L. H., Muthanna, H. H., Ahmed, S. O., Chitosan aerogel loaded with biogenic palladium nanoparticles CH/Pd NPs exert antibacterial activity and wound addressing application in vitro and in vivo against bacterial skin infections, *J. Mol. Struct.*, 1315, 138983 (2024).
<https://doi.org/10.1016/j.molstruc.2024.138983>
- Li, B., Wang, R., Shao, X., Shao, L. and Zhang, B., Synergistically enhanced photocatalysis from plasmonics and a co-catalyst in Au@ZnO–Pd ternary core–shell nanostructures, *Inorg. Chem. Front.*, 4, 2088–2096 (2017).
<https://doi.org/10.1039/C7QI00586E>
- Madhuree, K., Shipra, P., Ved, P. G., Chandra S. N. and Aradhana, M., A critical review on green approaches in shape and size evolution of metal nanoparticles and their environmental applications, *Environ. Nanotechnol. Monit. Manage.*, 20, 100895 (2023).
<https://doi.org/10.1016/j.enmm.2023.100895>
- Maha, A., Adel, A. I., Yousef, G. A., Nada, D. A. and Reda, M. M., Co₃O₄ Nanoparticles Accommodated Mesoporous TiO₂ framework as an Excellent Photocatalyst with Enhanced Photo-catalytic Properties, *Opt. Mater.*, 131, 112643 (2022),
<https://doi.org/10.1016/j.optmat.2022.112643>
- Mohammad, A. T. S. and Hassan, K., Green synthesis of silver nanoparticles with green tea extract from silver recycling of radiographic films, *Results Eng.*, 21, 101808 (2024).
<https://doi.org/10.1016/j.rineng.2024.101808>
- Mohammed, A. D., Nazila, O., Azlan, A. A., Pegah, M. K., Mushtak, T. S. A., Mahmood, S. J., Farhank, S. B., Baharak, M. and Mehran, G., Recent advances of plant-mediated metal nanoparticles: Synthesis, properties, and emerging applications for wastewater treatment, *J. Environ. Chem. Eng.*, 12(2), 112345 (2024).
<https://doi.org/10.1016/j.jece.2024.112345>
- Mohwes, N. M., Khawla, K. J. and Ayad, F. A., Photocatalytic degradation of Brilliant green dye by using ZnO–CdS/Pd nanocomposite, *Journal of Nanostructures*, 113951, 2251-7871 (2023).
- Monireh, G., Pedram, E., Zahra, R.G., Ahmad, N., Ali, D., Rezvan, K., Mina, A. and Tahoori, M., Green tea-mediated synthesis of silver nanoparticles: Enhanced anti-cancer activity and reduced cytotoxicity melanoma and normal murine cell lines, *Inorg. Chem. Commun.*, 161, 111989 (2024).
<https://doi.org/10.1016/j.inoche.2023.111989>
- Mouhaned, Y. A., Sattar, S. I. and Mohammed, A. M., A review on plant extract mediated green synthesis of zinc oxide nanoparticles and their biomedical applications, *Results Chem.*, 7, 101368 (2024).
<https://doi.org/10.1016/j.rechem.2024.101368>
- Nada, Y. T. and Reda, M. M., Sol-gel assembled MnCo₂O₄/rGO photocatalyst for enhanced production of aniline from photoreduction of nitrobenzene under visible light, *Ceram. Int.*, 48(9), 13216-13228 (2022).
<https://doi.org/10.1016/j.ceramint.2022.01.199>

- Pore, O. C., Fulari, A. V., Shejwal, R. V., Fulari, V. J. and Lohar, G. M., Review on recent progress in hydrothermally synthesized $\text{MCo}_2\text{O}_4/\text{rGO}$ composite for energy storage devices, *Chem. Eng. J.*, 426, 131544 (2021).
<https://doi.org/10.1016/j.cej.2021.131544>
- Prasad, P. R., Kanchi, S. and Naidoo, E. B., In-vitro evaluation of copper nanoparticles cytotoxicity on prostate cancer cell lines and their antioxidant, sensing and catalytic activity: One-pot green approach, *J. Photochem. Photobiol., B*, 161, 375-382 (2016).
<https://doi.org/10.1016/j.jphotobiol.2016.06.008>
- Priya, M., Premkumar, V. K. and Vasantharani, P., Sivakumar, G., Structural and electrochemical properties of ZnCo_2O_4 nanoparticles synthesized by hydrothermal method, *Vacuum*, 167, 307-312 (2019).
<https://doi.org/10.1016/j.vacuum.2019.06.020>
- Punyasamudram, S., Reddy, P. P., Ayyappa, B., Ravikumar, M., Kanchi, S. and Nagendra, K. P. V., Multifunctional characteristics of biosynthesized $\text{CoFe}_2\text{O}_4@Ag$ nanocomposite by photo-catalytic, antibacterial and cytotoxic applications, *Chemosphere*, 349, 140892 (2024).
<https://doi.org/10.1016/j.chemosphere.2023.140892>
- Rahman, A. M., Bayazeed, H. A., Heshu, S. R., Synthesis, cytotoxic, antibacterial, antioxidant activities, DFT, and docking of novel complexes of Palladium (II) containing a thiourea derivative and diphosphines, *J. Mol. Struct.*, 1295, 136519 (2024).
<https://doi.org/10.1016/j.molstruc.2023.136519>
- Rashmi, V. B., Green synthesis and Applications of Metal Nanoparticles - A Review Article, *Results in Chemistry*, 5, 2211-7156 (2023).
<https://doi.org/10.1016/j.rechem.2023.100832>
- Rosa, M. D. C., Jaime, V., Victor, R. J., Javier, Villa, E. L. and Adolfo, L. R., Green synthesis and characterization of silver nanoparticles using grape stalk extract, *J. Mol. Liq.*, 403, 124927 (2024).
<https://doi.org/10.1016/j.molliq.2024.124927>
- Rui, J., Shuangming, W., Mengying, D., Lifang, Z., Jing, C., Yi, Z., Mingzhe, Z., Yongming, S., Temperature-dependent formaldehyde and xylene dual selectivity in ZnCo_2O_4 sphere-like architectures, *Colloids Surf., A*, 675, 132042 (2023).
<https://doi.org/10.1016/j.colsurfa.2023.132042>
- Sabhat, F., Muhammad, N. A., Ihsan, H., Syed, W. A. S. and Muhammad, W., Green synthesis of cobalt ferrite and Mn doped cobalt ferrite nanoparticles: Anticancer, antidiabetic and antibacterial studies, *J. Trace Elem. Med. Biol.*, 80, 127292 (2023).
<https://doi.org/10.1016/j.jtemb.2023.127292>
- Sandhya, P., Reddy Prasad, P., Ayyappa, B., Kanchi, S. and Jyothi, S., Nagendra Kumar, P.V., Biosynthesis of $\text{ZnFe}_2\text{O}_4@Ag$ hybrid nanocomposites for degradation of 2,4-Dichlorophenoxyacetic acid herbicide, *Chem. Phys. Impact*, 7, 100282 (2023).
<https://doi.org/10.1016/j.chphi.2023.100282>
- Sebastian, C. J., Subramani, S., Dae, J. M., Sathyanarayanan, S., Joon, Y. K., Gnanaprakasam, J., Krishnan, V., Shivraj, M., Goo, K., Pildo, J., Gibum, K., Kyoungsuk, J., Jung, K. K., Kootak, H., Yong, I. P., Tae-Hoon, K., Jaeyeong, H. and Uk, S., Defect engineered ternary metal spinel-type Ni-Fe-Co oxide as bifunctional electrocatalyst for overall electrochemical water splitting, *J. Colloid Interface Sci.*, 663, 566-576 (2024).
<https://doi.org/10.1016/j.jcis.2024.02.042>
- Seung, J. L., Hyeon, J. J., Ravindranadh, K., Seung, H. L., Malathi, A., Ju, H. K. and Myong, Y. C., ZnO supported Au/Pd bimetallic nanocomposites for plasmon improved photo-catalytic activity for methylene blue degradation under visible light irradiation, *Appl. Surf. Sci.*, 496, 143665 (2019).
<https://doi.org/10.1016/j.apsusc.2019.143665>
- Shankar, G. R., Balkrishna, J. L., Utilization of spray pyrolyzed porous nickel cobaltite electrode as an advanced material for $\text{NiCo}_2\text{O}_4@Graphite$ asymmetric supercapacitor device, *Inorg. Chem. Commun.*, 161, 112099 (2024).
<https://doi.org/10.1016/j.inoche.2024.112099>
- Siyuan, W., Ding, C., Qiu H., Ying G., Yucheng, C., Guanlin, R. and Zhao, L., Surface functionalization of metal and metal oxide nanoparticles for dispersion and tribological applications – A review, *J. Mol. Liq.*, 389, 122821 (2023).
<https://doi.org/10.1016/j.molliq.2023.122821>
- Sunaina, S., Prakash, C., Aman, J., Fabrication of ultrahigh supercapacitor device based on $\text{ZnCo}_2\text{O}_4@MnO_2$ with porous nanospheres decorated on flower-shaped structure, *J. Energy Storage*, 71, 108209 (2023).
<https://doi.org/10.1016/j.est.2023.108209>
- Tholkappiyan, R., Fathalla, H., Fabrication of dual-1D/2D shaped $\text{ZnCo}_2\text{O}_4\text{-ZnO}$ electrode material for highly efficient electrochemical supercapacitors, *J. Phys. Chem. Solids*, 188, 111915 (2024).
<https://doi.org/10.1016/j.jpcs.2024.111915>
- Uyiosa, O. A. and Otolorin, A. O., Green synthesis of metal oxide nanoparticles, and their various applications, *J. Hazard. Mater. Adv.*, 13, 100401 (2024).
<https://doi.org/10.1016/j.hazadv.2024.100401>
- Varunamugi, R., Mathu, M. K., Arun, P. C., Sathyaseelan, T., Sathiyaraj, S., Prakash, T., Vandamar, P. R., Ranjith, K. E. and Aruna, D. N., Synthesis and characterization of Co_3O_4 , CuO and NiO and nanoparticles: Evaluation of structural, vibrational, morphology and thermal properties, *Phys. Lett. A*, 512, 129574 (2024).
<https://doi.org/10.1016/j.physleta.2024.129574>
- Vinod, K., Naveen, K. K., Tiwari, S. K., Davender, S. and Bijender, S., Green synthesis of iron nanoparticles: Sources and multifarious biotechnological applications, *Int. J. Biol. Macromol.*, 253(4), 127017 (2023).
<https://doi.org/10.1016/j.ijbiomac.2023.127017>

Zikirina, A., Kadyrzhanov, K. K., Kenzhina, I. E., Kozlovskiy, A. L. and Zdorovets, M. V., Study of defect formation processes under heavy ion irradiation of ZnCo₂O₄ nanowires, *Opt. Mater.*, 118, 111282 (2021).
<https://doi.org/10.1016/j.optmat.2021.111282>